RSC Advances

ROYAL SOCIETY OF CHEMISTRY

www.rsc.org/advances

Surface charge modification in improvement of photocatalytic H_2 production over $La_2Ti_2O_7$/graphene nanocomposite

Sujuan Hu, Bo Chi,* Jian Pu and Li Jian

Table of Contents

An intimate interfacial contacted $La_2Ti_2O_7$/graphene nanocomposite shows enhanced photocatalytic H_2 production rate and photo–electrochemistry activity.

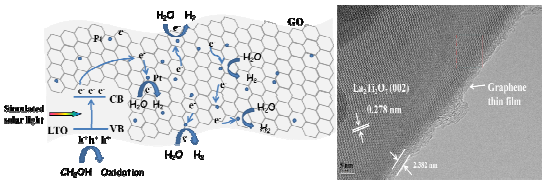

Journal Name

RSCPublishing

ARTICLE

Surface charge modification in improvement of photocatalytic H_2 production over $La_2Ti_2O_7$/graphene nanocomposite

Cite this: DOI: 10.1039/x0xx00000x

Received 00th January 2014,
Accepted 00th January 2014

DOI: 10.1039/x0xx00000x

www.rsc.org/

Sujuan Hu, Bo Chi,* Jian Pu and Li Jian

An intimate interfacial contact and large contact area $La_2Ti_2O_7$/graphene (GR) nanocomposite is synthesized by a facile electrostatic self−assembly approach. The nanocomposite is characterized by X−ray diffraction (XRD), scanning electron microscopy (SEM), transmission electron microscopy (TEM), UV−Vis diffuse reflectance spectra, X−ray photoelectron spectroscopy (XPS), Fourier transform infrared spectroscopy (FT−IR), Raman spectra and photoluminescence spectra (PL). The $La_2Ti_2O_7$/GR nanocomposite exhibits the highest H_2 production rate when used in photocatalytic water splitting, as improved by 5.7 and 4.9 times relative to pure $La_2Ti_2O_7$ and $La_2Ti_2O_7$/GR−H that prepared without surface charge modification, respectively. In addition, the transient photocurrent responses and electrochemical impedance spectra (EIS) results indicate that the $La_2Ti_2O_7$/GR nanocomposite exhibits more effective separation of photogenerated electron–hole pairs and faster interfacial electron transfer as compared with pure $La_2Ti_2O_7$ nanosheets and $La_2Ti_2O_7$/GR−H nanocomposite. The enhanced photocatalytic H_2 production rate and photo–electrochemistry activity can be ascribed to the intimate interfacial contact and large contact area between $La_2Ti_2O_7$ nanosheets and GR which help to make full use of the electron conductivity of GR for transferring the photogenerated electrons, prolonging the lifetime of charge carriers and improving the rate of water splitting to form H_2.

1. Introduction

Hydrogen (H_2) as a clean, no carbon emission and high energy density (140 MJ Kg^{-1}) fuel has been considered as the major energy of the future.[1-3] The traditional production of H_2 is through consuming non-renewable and increasingly depleted fossil fuel and this method is seriously limited by its low productivity, high cost and environment−unfriendly. Photocatalytic water−splitting for H_2 evolution has become a promising approach to realize the solar−fuel conversion since Fujishima and Honda first reported the photoelectrochemical splitting of water into H_2 and O_2 on a TiO_2 semiconductor electrode in 1972.[4−7] However, the rapid recombination of photogenerated electron-hole pairs in semiconductors restricts the enhancement of their photocatalytic H_2 production activity.[8−10] To overcome this shortcoming and enhance photocatalytic H_2 production efficiency, many studies have been devoted to reduce the recombination rate of charge carriers by coupling photocatalysts with other materials, such as noble metals, semiconductors or carbon materials.[11−15] Recently, graphene (GR, RGO) as an excellent functional carbon material has received comprehensively research because of its unique two−dimensional (2D) network of hexagonal structured sp^2–hybridized structure.[16−20] It has been demonstrated that coupling semiconductor with a conjugative π structure graphene is an effective means of improving photocatalytic H_2 production efficiency of the semiconductor. And the improvement can ascribe to the excellent electron conductivity of GR which acts as an electron reservoir to accept and shuttle photogenerated electrons over semiconductor.[21-24] For example, Wang et al. reported that a RGO/AgBr composite exhibited enhanced photocatalytic H_2 evolution compared to bare AgBr.[25] Dong et al. measured that mean life time of photogenerated electron−hole pairs of RGO−TiO_2 nanocomposite was prolonged from $\sim10^{-7}$ to $\sim10^{-5}$ s in comparison with that of TiO_2.[26]

(110) layered-structure perovskites, such as $M_2N_2O_7$ (M = Ca, Sr, La; N = Nb, Ti), have received increasing attention because of their unique electronic configuration, high chemical resistance and interlayer spatial structure enabling the use of different reaction sites for water oxidation and reduction.[27, 28] Among the perovskites, lanthanum titanate ($La_2Ti_2O_7$, LTO) has received major attention because of its efficiency in photocatalytic H_2 production from water splitting.[29−31] The conventional preparation methods of $La_2Ti_2O_7$ are solid−state reaction (SSR) and sol−gel methods. However, neither of these methods is convenient or economical. In addition, the particles obtained are large with the low undesirably specific surface areas. These characteristics are not favorable to efficient and low-cost photocatalytic H_2 production activity. For an efficient photocatalyst, a large specific surface area is desirable. To obtain such an area for the catalysts reported in this work, a hydrothermal method was used

to prepare two-dimensional $La_2Ti_2O_7$ nanosheets because this morphology is more effective than zero-dimensional $La_2Ti_2O_7$ particles from the viewpoint of the mobility and recombination rate of charge carriers.

Interfacial contact and contact area between GR and a semiconductor are crucial to influencing electrons transfer efficiency from the semiconductor to GR.[32–36] Intimate interfacial contact and large contact area help to make full use of the electron conductivity of GR for promoting transfer rate of photogenerated electrons and prolonging life span of the charge carriers, thus result in the improvement of catalyst's photoactivity for H_2 evolution.[37, 38]

Many attempts have been tried to modify $La_2Ti_2O_7$ photocatalyst for applying in degradation of organic dyes and H_2 production from water−splitting.[39–42] However, few studies have been conducted on $La_2Ti_2O_7$/GR nanocomposite. Herein, to take advantage of graphene as electrons acceptor and transporter effectively, we used a facile electrostatic self−assembly approach to prepare intimate interfacial contact and large contact area $La_2Ti_2O_7$/GR nanocomposite and investigate the synergistic effects of the GR and $La_2Ti_2O_7$ combination on the photocatalytic H_2 production activity. The $La_2Ti_2O_7$/GR nanocomposite exhibits higher photocatalytic H_2 production activity and photo−electrochemistry performance than those of pure $La_2Ti_2O_7$ nanosheets. For comparison, both of the property measurements are conducted on LTO/GR−H nanocomposite that prepared without surface charge modification. The results revealed that spontaneous attraction of electrostatic forces helps to reinforce the interfacial contact between $La_2Ti_2O_7$ nanosheets and GR and the intimate interfacial contact helps to make full use of the electron conductivity of GR for transferring the photogenerated electrons and prolonging the lifetime of charge carriers and thus results in improvement of the photoactivities.

2. Experimental

2.1. Materials

All chemicals were of analytical grade and purchased from Sinopharm Chemical Reagent Co., Ltd. without further purification before use. High–purity deionized (DI) water was used throughout our experiments.

2.2 Preparation of graphene oxide (GO) nanosheets

Graphite oxide (GO) nanosheets were synthesized by chemical exfoliation of graphite powder according to a modified Hummers' method.[43, 44] Specifically, 2.0 g of graphite powder was added to 46 mL concentrated H_2SO_4 in an ice−bath, after which 6.0 g of $KMnO_4$ was gradually added under vigorous stirring. The temperature of the mixture was maintained below 20 °C during this process. The mixture was then further stirred at 35 °C for 30 min, after that 92 mL distilled water was added to the system, followed by stirring the resultant mixture at 98 °C for 15 min. The reaction was terminated by adding 280 mL of distilled water, which was followed by 10 mL of 30 % H_2O_2 solution. The solid product was separated by centrifugation and washed repeatedly with 5 % HCl solution until sulfate could not be detected with $BaCl_2$. Then the sample was dried in a vacuum oven at 40 °C overnight.

2.3 Synthesis of $La_2Ti_2O_7$ nanosheets.

$La_2Ti_2O_7$ nanosheets were prepared by a hydrothermal method.[15] Specifically, 5 mmol $Ti(OBu)_4$ was mixed in 50 mmol CH_3COOH while stirring vigorously for 30 min and 5 mmol $La(NO_3)_3{\cdot}6H_2O$ was dissolved in 10 mL deionized water. This was added dropwise to the $Ti(OBu)_4/CH_3COOH$ mixture, giving a clear aqueous solution. 30 mL 1.8 M NaOH solution was then added to this solution. The resulting solution was transferred to a 100 mL Teflon-lined stainless steel autoclave and heat-treated at 200 °C for 24 h. The product was collected after centrifugation, washed with water and ethanol repeatedly, and then dried at 80 °C for 12 h.

2.4 Synthesis of $La_2Ti_2O_7$/GR nanocomposite.

$La_2Ti_2O_7$/GR nanocomposite was prepared by a electrostatic self−assembly approach assisted with a hydrothermal reduction method, as shown in Scheme 1.[45] In detail, 0.2 g of $La_2Ti_2O_7$ was first dispersed in 200 mL ethanol by sonication for 30 min. Then, 2 mL (aminopropyl)trimethoxysilane APTMS was added into the above mixture and heated at 100 °C for 4 h under vigorously stirring. The redundant APTMS were washed with ethanol. Self−negatively charged GO suspension (0.2 mg/mL) was added into positively charged functionalized $La_2Ti_2O_7$ dispersion solution and weight ratio of GO to $La_2Ti_2O_7$ is 5 %. After mixing for 30 min, the precipitate was washed again with deionized water. A hydrothermal method was adopted for reduction of GO to GR in a 100 mL Teflon−lined stainless steel vessel at 120 °C for 12 h. The precipitate was collected after centrifugation, washed and then dried at 80 °C for 12 h. In addition, the samples of $La_2Ti_2O_7$/GR with different weight ratios of GO (1 wt% and 10 wt%) were also prepared by the same method. To investigate the influence of surface charge modification to the interfacial interaction between GR and $La_2Ti_2O_7$ nanosheets, the sample without surface charge modification was prepared according to the above processes just omitted the process of APTMS−modified $La_2Ti_2O_7$ and the sample was labelled as LTO/GR−H.

2.5 Deposition of Pt cocatalyst on photocatalyst.

Deposition of Pt (1.0 wt%) cocatalyst on photocatalyst surface was achieved through typical in−situ photoreduction of H_2PtCl_6 with UV−light irradiation.[46] 0.2 g of photocatalyst was suspended in 200 mL of aqueous solution containing 20 %(v/v) methanol as the sacrificial donor. The appropriate amount of H_2PtCl_6 was added to the mixture. Following this, the suspension was stirred and purged with N_2 continually to ensure anaerobic conditions. After that, the suspension was illuminated with UV light for 4 h. The precipitate was collected by centrifugation and dried at 80 ºC for 12 h.

2.6 Characterization

X−ray diffraction (XRD) measurements were carried out using an X−ray diffractometer (XRD, X'Pert pro. PANalytical B.V) with Cu Kα radiation. Both scanning electron microscopy (FE−SEM, FEI, Sirion 200) and transmission electron microscopy (TEM, JEM−2100F) were used to characterize the morphologies of the samples. X−ray photoelectron spectroscopy (XPS) was performed on a KRATOS AXIS165 X−ray photoelectron spectrometer. The

UV−Vis diffuse reflectance spectra were recorded with a Perkin−Elmer Lambda 35 UV−Vis spectrophotometer. The Fourier transform infrared spectroscopy (FT−IR) was recorded on a Bruker VERTEX 70. The Raman spectra and photoluminescence (PL) spectra were recorded on a laser confocal Raman microspectroscopy (LabRAM HR800, Horiba JobinYvon) with excitation wavelengths of 536 nm and 325 nm, respectively.

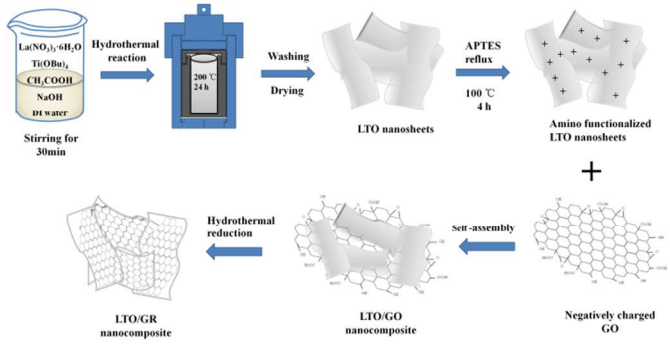

Scheme 1 Illustration for preparation of $La_2Ti_2O_7$/GR nanocomposite.

2.7 Photocatalytic activity

The photocatalytic H_2 production experiments were performed in a quartz reactor under solar light irradiation at ambient temperature and atmospheric pressure. A 500 W Xe lamp (100 mW cm^{-2}, CHF−XM 500, Beijing Trusttech Co., Ltd.) was used as the light source. In a typical photocatalytic experiment, 0.1 g of photocatalyst was suspended in 150 mL of aqueous solution containing 25 %(v/v) methanol. Before all photocatalytic H_2 production experiments, the reaction vessel was evacuated for 30 min to remove dissolved oxygen and ensure the anaerobic conditions. Throughout the experiment 1 mL of gas was sampled intermittently and hydrogen content was analyzed using a gas chromatograph (DongXi GC−A5000, with high purity Ar as carrier gas) equipped with a thermal conductivity detector.

2.8 Photo−electrochemical measurement

Photocurrents and electrochemical impedance spectra (EIS) were measured using an electrochemical analyzer (Zennium, Zahner) with a standard three−electrode system using the prepared samples as the working electrodes, a platinum plate as the counter electrode and a Ag/AgCl (saturated KCl) as the reference electrode in 1 M Na_2SO_4 aqueous solution. A 500 W Xe lamp (100 mW cm^{-2}, CHF−XM 500, Beijing Trusttech Co., Ltd.) was used as the light source. For the preparation of the working electrodes, 0.2 g of the photocatalyst was ground with 0.06 g polyethylene glycol (PEG, molecular weight: 20000 Da) and 0.5 mL water to make a slurry. The slurry was subsequently coated onto a 2 cm×1.5 cm FTO glass electrode by the doctor−blade method. The resulting electrodes were dried and calcined at 450 ºC for 30 min. All electrodes studied had a similar film thickness (10~11 μm).[47, 48]

3. Results and discussion

The XRD patterns of pure LTO, LTO/GR and LTO/GR−H nanocomposites are shown in Fig. 1. It can be found that the pure LTO prepared through a hydrothermal method shows a monoclinic phase with a perovskite structure belonging to the $P2_1$ space group (JCPDS 01-081−1066). The peaks located at ca. 28.20º, 30.03º, 32.39º and 33.09º can be indexed to (040), (211), (002) and (012) crystal planes of the monoclinic $La_2Ti_2O_7$ phase and no other impurity phase is detected. For LTO/GR and LTO/GR−H nanocomposites, they show similar XRD patterns to pure LTO and no GR diffraction peak is observed. This might be due to the small amount and low diffraction intensity of GR in the nanocomposites.

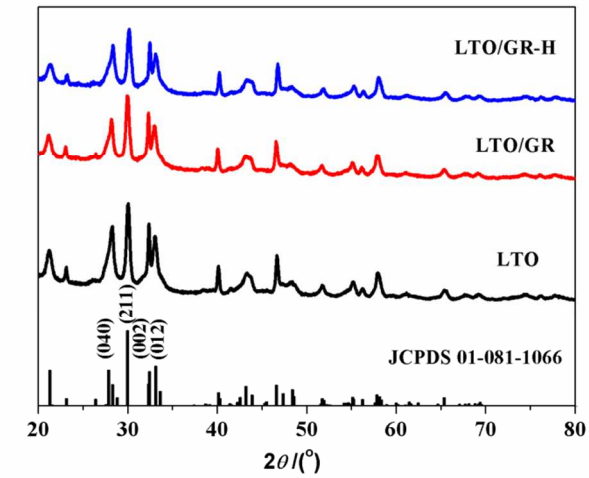

Fig. 1 XRD patterns of LTO, LTO/GR and LTO/GR−H nanocomposites.

The UV−vis diffuse reflectance spectra (DRS) of pure LTO, LTO/GR and LTO/GR−H nanocomposites are presented in Fig.2. The DRS of LTO/GR with different weight ratios of GR (1 wt% and 10 wt%) are shown in Fig. S1. For pure LTO, the DRS spectrum presents a steep absorption edge at approximately 350 nm, which can be assigned to the intrinsic bandgap absorption of LTO (3.8 eV). After compositing with graphene, the absorption intensities in visible−light region are all improved. This is mainly due to the background absorption of GR in the visible light region. Besides, the absorption intensity in visible−light region is strengthened along with the increase of GR amount.

The photocatalytic activities of pure LTO, LTO/GR and LTO/GR−H nanocomposites were evaluated by measuring H_2 production from water splitting under 500 W Xe lamp irradiation, as shown in Fig. 3(A). To improve the photocatalytic H_2 production, 1 wt% Pt cocatalyst was loaded onto the photocatalyst surfaces to provide active sites for the reaction. The photocatalytic H_2 evolution rates over pure LTO is only 10.59 μmol h^{-1} g^{-1} and H_2 evolution rates are distinctly enhanced to 60.45 μmol h^{-1} g^{-1} after compositing with 5 wt% graphene through electrostatic self−assembly approach. However, the performance decreases to 8.47 μmol h^{-1} g^{-1}, even lower than that of pure LTO, for LTO composite with 10 wt% graphene (Fig. S2). This is due to the excessive amounts of graphene absorbing a certain amount of light and weakening the transmittance of incident light.

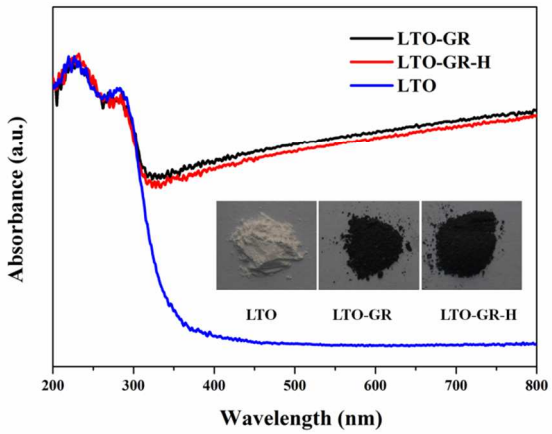

Fig. 2 UV-vis diffuse reflectance spectra of LTO, LTO/GR and LTO/GR−H nanocomposites.

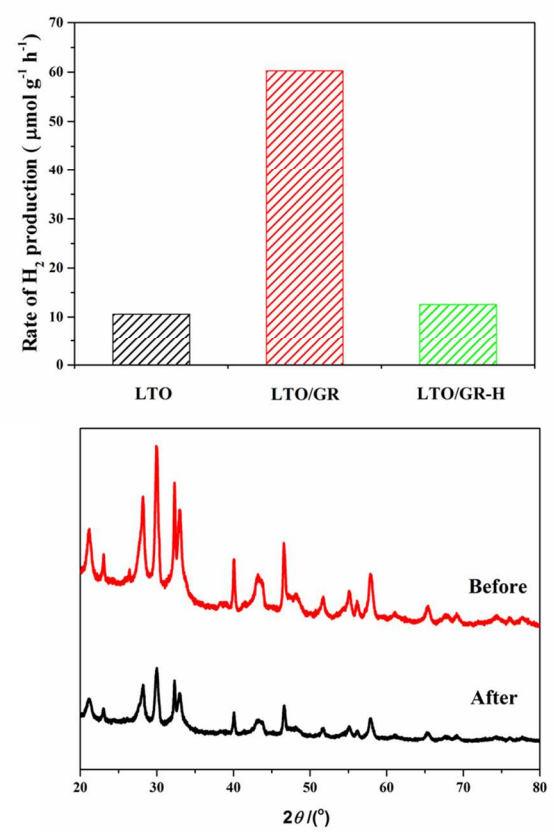

Fig. 3 Effect of LTO, LTO/GR and LTO/GR−H nanocomposites on the photocatalytic H_2 evolution rates under 500 W Xe lamp irradition (A) and XRD patterns of LTO/GR before and after reaction (B).

However, for LTO/GR−H nanocomposite which prepared without surface charge modification, the photocatalytic H_2 evolution rate is 12.41 μmol h^{-1} g^{-1}, slightly higher than that of pure LTO but far below than that of LTO/GR nanocomposite. The crystal structure of LTO/GR nanocomposite after photoreaction is essentially similar to the unused one (Fig. 3 (B)). No obvious deviation in peaks location indicating LTO/GR nanocomposite owns crystalline structure stability. The photostability of Pt (1 wt%) loaded LTO/GR nanocomposites, which is investigated in two runs of accumulatively 8 h (Fig. S3). The average H_2 generation rate over Pt (1 wt%) loaded LTO/GR nanocomposite is about 47.72 μmol g^{-1} h^{-1} in the first run of 8 h photocatalytic reaction, and then slightly decreases to 44.44 μmol g^{-1} h^{-1} in the second. The performance degradation is about 6.9 %, indicating the photocatalyst with good stability.

To explore and understand the origins of the improved photocatalytic H_2 production of LTO/GR nanocomposite, a series of characterizations have been conducted. The morphologies of LTO, LTO/GR and LTO/GR−H nanocomposites are shown in Fig. 4. It is clear to see that pure LTO shows irregular thin nanosheets (Fig. 4A). Fig. 4(B) and 4(C) are typical SEM and HRTEM images of LTO/GR nanocomposite. It is not easy to be perceived but through careful observation still can be found that graphene thin layers are smoothly and tightly covered onto the surface of LTO nanosheets and some wrinkles caused by GR thin layers are marked with white dotted line in Fig. 4(B). For better observing the interfacial contact between LTO nanosheets and GR, HRTEM image is displayed, as shown in Fig. 4(C). The interplanar distance of 0.278 nm is in good agreement with the d-spacing of the (002) plane of a monoclinic $La_2Ti_2O_7$. The graphene thin film ca. 2.382 nm intimately contacts with LTO and no obvious lattice distortions in the interfacial region between LTO and graphene. However, the case is quite different for LTO/GR−H nanocomposite (Fig. 4(D)). The GR surfaces do not effectively integrate with LTO nanosheets and the interfacial contact area is relatively small. The morphology of LTO in LTO/GR and LTO/GR−H nanocomposites is similar to pure LTO nanosheets, indicating the difference in photocatalytic H_2 production over these photocatalysts cannot be caused by the change of LTO morphology. Therefore, we can understand the large distance in photocatalytic H_2 production is caused by the introduction of graphene and different compositing methods. LTO/GR nanocomposite has a process of surface charge modification of LTO nanosheets and this process leads to LTO nanosheets electrostatic assembled with negatively charged GO, results in intimate interfacial contact and large contact area. This intimate interfacial contact and large contact area help to make full use of the electron conductivity of graphene for transferring the photogenerated electrons and prolonging the lifetime of charge carriers that are favorable to high photocatalytic H_2 production. On the contrary, tough and poor interfacial contact in LTO/GR−H would not take advantage of graphene on electrons transfer.

XPS is used to further investigate the chemical nature and interaction between graphene and LTO nanosheets. The full spectra (Fig. 5A) show that elements Ti, La, O and C exist in LTO/GR nanocomposite. The corresponding high−resolution XPS spectra of C 1s, O 1s, La 3d and Ti 2p are shown in 5C−5F, respectively. Three peaks, 284.97, 286.18 and 289.94 eV, are observed in C 1s core level spectra and there are ascribed to C−C (sp^2 bonded carbon), C−O (epoxy/hydroxyl) and O−C=O (carboxyl), respectively (Fig. 5B).[49] Fig. 5C presents the high−resolution XPS spectra for O 1s. Two oxygen signals are observed at 532.97 and 530.93 eV, which can be attributed to surface adsorption oxygen and lattice oxygen, respectively.[50] Fig. 5D reveals the high resolution XPS spectra for La 3d. Seven peaks are observed in the La 3d core level spectra and all of these peaks originate from the spin−orbital splitting of the $3d_{5/2}$ and $3d_{3/2}$ states of La (□).[51] The peaks located at 465.33 and 459.60 eV correspond to Ti $2p_{1/2}$ and Ti $2p_{3/2}$, respectively (Fig. 5E).[52]

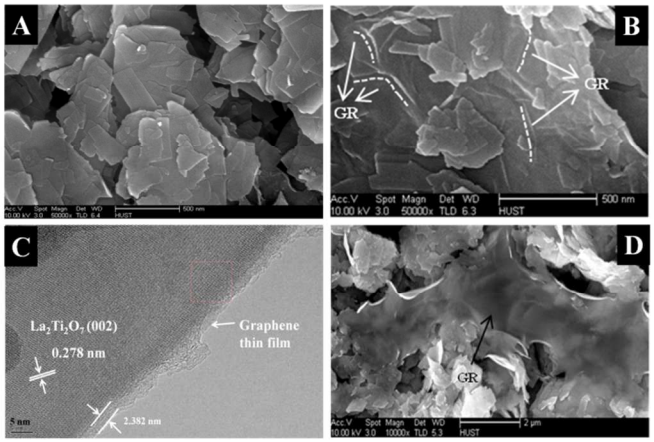

Fig. 4 Typical SEM image of LTO (A), SEM and HRTEM images of LTO/GR nanocomposite (B) and (C) and SEM image of LTO/GR−H nanocomposite (D).

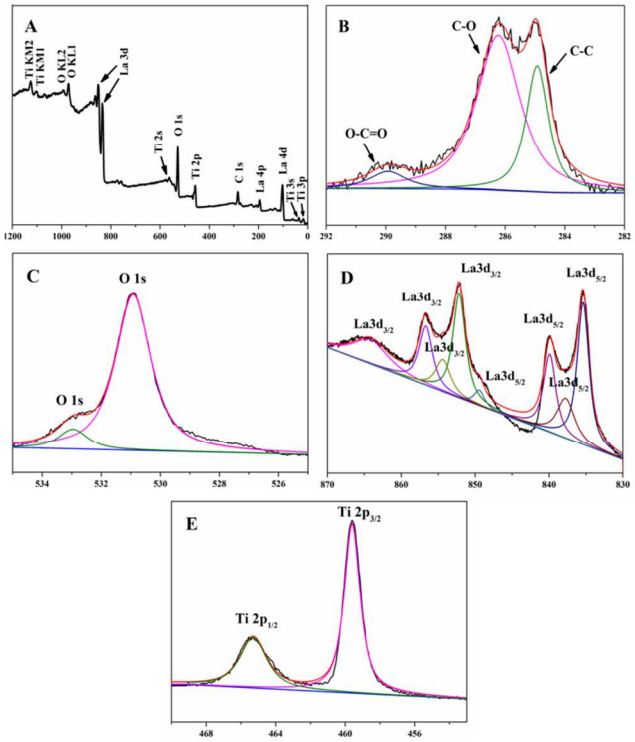

Fig. 5 XPS spectra of LTO/GR nanocomposite: (A) Fully scanned spectra, (B) C 1s, (C) O 1s, (D) La 3d and (E) Ti 2p high−resolution XPS spectra.

Raman spectroscopy is an efficient tool for characterization of carbon materials. As seen in Fig. 6, two characteristic peaks in the spectrum of GO are named as the D band (1350 cm^{-1}) and the G band (1590 cm^{-1}) and the two peaks are also appeared in LTO/GR and LTO/GR−H nanocomposites.[53] The D band is ascribed to local defects or disorders, while the G band arises from the sp^2 hybridized graphene domains.[54] Intensity ratio (I_D/I_G) of the D band to the G band in GO is ca. 0.46, while the I_D/I_G of LTO/GR and LTO/GR−H nanocomposites are ca. 0.77 and 0.86, respectively. The increase of I_D/I_G value is attributed to reduction and restoration of the sp^2 network of GO after hydrothermal treatment, which suggests successful reduction of GO to graphene.[55, 56] In addition, slight red−shifts of the D band and the G band in LTO/GR nanocomposite as compared with GO could be caused by the interaction between LTO nanosheets and graphene.

To further verify the interaction between LTO nanosheets and graphene, FT−IR is characterized, as shown in Fig. 7. Five characteristic peaks at ca. 1049, 1269, 1400, 1620 and 1736 cm^{-1} in GO spectrum are caused by C–O stretching vibrations of epoxy groups, C–O stretching vibrations of phenolic C–OH, O–H deformation vibrations of tertiary C–OH, H–O–H bending band of adsorbed H_2O molecules or skeletal vibrations of unoxidized C–C bonding and C=O stretching vibrations of COOH groups, respectively.[57, 58] However, a dramatic decrease occurred in these peaks intensities for LTO/GR and LTO/GR–H nanocomposites, indicating the reduction of GO to graphene. In addition, a new peak at ca. 1548 cm^{-1} is observed which is caused by the skeletal vibration absorption of graphene.[59]

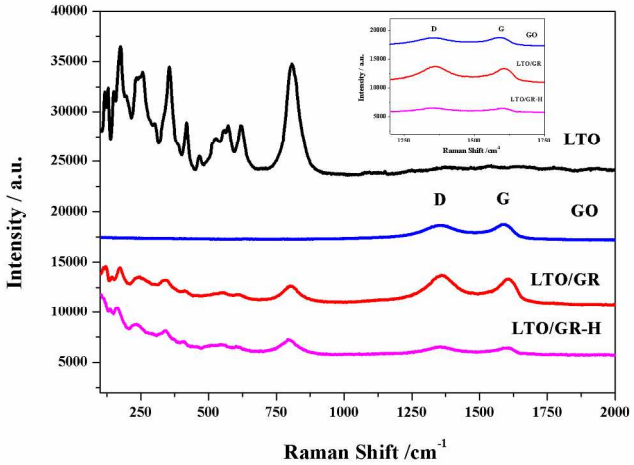

Fig. 6 Raman spectra of LTO, GO, LTO/GR and LTO/GR−H nanocomposites.

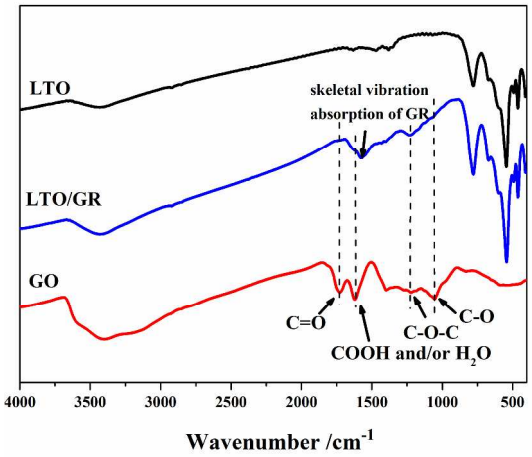

Fig. 7 FTIR spectra of LTO, GO and LTO/GR nanocomposite.

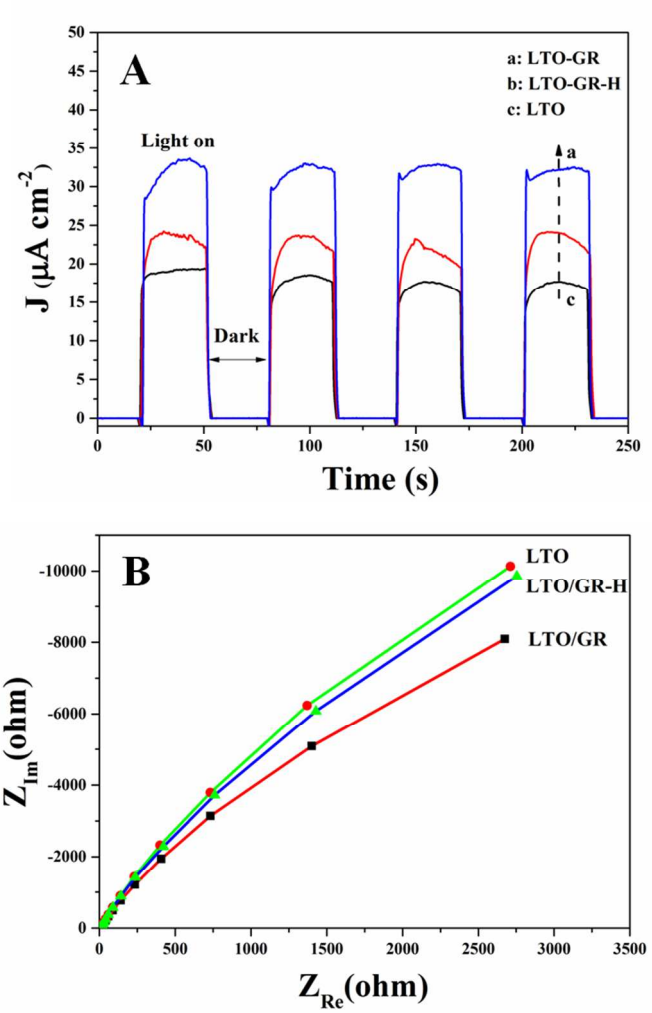

Fig. 8 Transient photocurrent responses and electrochemical impedance spectra (EIS) Nyquist plots of LTO, LTO/GR and LTO/GR−H nanocomposites under simulated solar light in 1 M Na_2SO_4 aqueous solution.

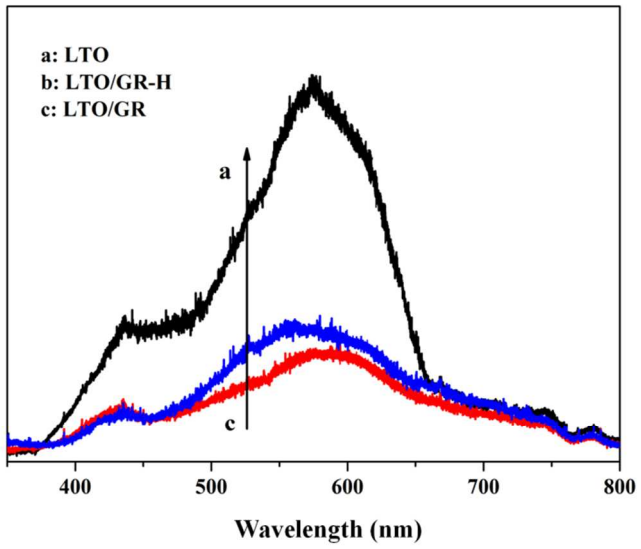

Fig. 9 Photoluminescence (PL) spectra of LTO, LTO/GR and LTO/GR−H nanocomposites.

Photo−electrochemical measurements are used to study the interfacial electrons transfer of photocatalyst. In our experiments, transient photocurrent responses (J−t) and electrochemical impedance spectra (EIS) were performed to better understand the photogenerated carrier separation of LTO/GR nanocomposite (Fig. 8). All of samples possess relatively stable photocurrent responses (Fig. 8(A)), suggesting that work electrodes are stable and photoresponse is quite reversible.[60] The photocurrent density obtained over LTO/GR nanocomposite is obviously enhanced compared to that of LTO/GR−H and pure LTO. Photocurrent is formed mainly by transferring photogenerated electrons to the counter electrode, the higher photocurrent over LTO/GR indicates more effective separation and longer lifetime of photogenerated electrons on it. Besides, electrochemical impedance spectra (EIS) Nyquist analysis is performed from 0.1 Hz to 3000 Hz to investigate the interfacial electrons transfer (Fig. 8(B)). As known, the high−frequency arc corresponds to the charge transfer limiting process and can be attributed to the charge transfer resistance at the contact interface between the electrode and electrolyte solution and the charge transfer resistance can be directly measured by semicircle diameter.[61-63] It can be observed that the arc of LTO/GR prepared through electrostatic self−assembly approach is smaller than that of LTO and LTO/GR−H in the high−frequency region implies that LTO/GR nanocomposite has faster interfacial electron transfer and more effective separation of photogenerated electron–hole pairs, which is in according with its higher photocatalytic H_2 production and transient photocurrent responses. Then, photoluminescence (PL) spectra of LTO, LTO/GR and LTO/GR−H nanocomposites are measured (Fig. 9). LTO/GR displays dramatically diminished PL intensity as compared with LTO and LTO/GR−H, suggesting that recombination rate of photogenerated electron−hole pairs is efficiently suppressed. These results are also well in accordance with photo−electrochemical performances and photocatalytic H_2 production activities.

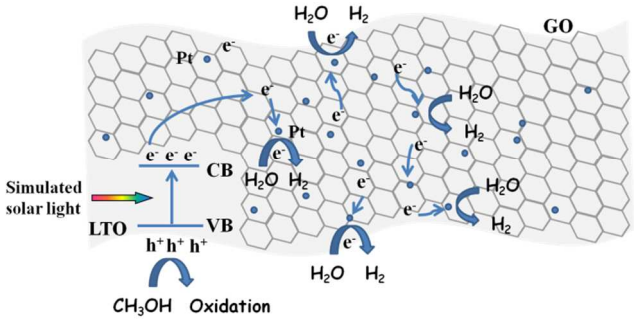

Fig. 10 The proposed photocatalytic H_2 evolution mechanism over $La_2Ti_2O_7$/GR nanocomposite under simulated solar light irradiation.

On the basis of the above analysis and discussion, it can be concluded that the intimate interfacial contact and large contact area between $La_2Ti_2O_7$ nanosheets and graphene are crucial to improving photo−electrochemical performance and photocatalytic H_2 production activity. Because the reduction potential of GR/GR•− is about −0.08 eV, well interfacial contact and large contact area between $La_2Ti_2O_7$ nanosheets and graphene could effective promote

photogenerated electrons transfer from $La_2Ti_2O_7$ to graphene, and then these electrons are readily trapped by Pt particles to reduce H_2O to H_2. Meanwhile, the photogenerated holes are oxidized by methanol, as shown in Fig. 10.

4. Conclusions

We adopted a facile electrostatic self−assembly approach to prepare well interfacial contact and large contact area of $La_2Ti_2O_7$/GR nanocomposite. $La_2Ti_2O_7$/GR nanocomposite displays higher photocatalytic H_2 production activity and photo−electrochemical performance than those of $La_2Ti_2O_7$ and $La_2Ti_2O_7$/GR−H nanocomposite that prepared without surface charge modification. The well photocatalytic activities of $La_2Ti_2O_7$/GR nanocomposite can be ascribed to intimate interfacial contact and large contact area between $La_2Ti_2O_7$ nanosheets and graphene that help to make full use of the excellent electron conductivity of graphene for transferring the photogenerated electrons and prolonging the lifetime of charge carriers. Electrostatic self−assembly approach plays a significant role in constructing high photocatalytic H_2 production GR−based semiconductor.

Acknowledgements

This work is supported by the National Natural Science Foundation of China (50902056). The authors would like to thank the Materials Characterization Center of Huazhong University of Science and Technology for measurement assistance.

Notes and references

Center for Fuel Cell Innovation, State Key Laboratory of Materials Processing and Die and Mould Technology, School of Materials Science and Engineering, Huazhong University of Science and Technology, Wuhan 430074, China. Fax: + 86 27 87558142; Tel: + 86 27 87558142; E-mail: chibo@hust.edu.cn (B. Chi)

[1] A. J. Bard and M. A. Fox, *Acc. Chem. Res.*, 1995, **28**, 141.
[2] Y. Amao, *ChemCatChem*, 2011, **3**, 458.
[3] J. Barber and B. Andersson, *Nature*, 1994, **370**, 31.
[4] A. Fujishima and K. Honda, *Nature*, 1972, **238**, 37.
[5] D. E. Scaife, *Solar Energy*, 1980, **25**, 41.
[6] K. Rajeshwar, *J. Phys. Chem. Lett.*, 2011, **2**, 1301.
[7] J. Tang, J. R. Durrant and D. R. Klug, *J. Am. Chem. Soc.*, 2008, **130**, 13885.
[8] W. Choi, A. Termin and M. R. Hoffmann, *Angew. Chem.*, 1994, **106**, 1148.
[9] K. Domen, A. Kudo, T. Onishi, N. Kosugi and H. Kuroda, *J. Phys. Chem.*, 1986, **90**, 292.
[10] V. H. Houlding and M. Grätzel, *J. Am. Chem. Soc.*, 1983, **105**, 5695.
[11] T. Hirakawa and P. V. Kamat, *J. Am. Chem. Soc.*, 2005, **127**, 3928.
[12] V. Subramanian, E. E. Wolf and P. V. Kamat, *J. Am. Chem. Soc.*, 2004, **126**, 4943.
[13] S. H. Elder, F. M. Cot, Y. Su, S. M. Heald, A. M. Tyryshkin, M. K. Bowman, Y. Gao, A. G. Joly, M. L. Balmer, A. C. Kolwaite, K. A. Magrini and D. M. Blake, *J. Am. Chem. Soc.*, 2000, **122**, 5138.
[14] T. Tatsuma, S. Saitoh, P. Ngaotrakanwiwat, Y. Ohko and A. Fujishima, *Langmuir*, 2002, **18**, 7777.
[15] K. Woan, G. Pyrgiotakis and W. Sigmund, *Adv. Mater.*, 2009, **21**, 2233.
[16] S. Guo and S. Dong, *Chem. Soc. Rev.*, 2011, **40**, 2644.
[17] A. K. Geim and K. S. Novoselov, *Nat. Mater.*, 2007, **6**, 183.
[18] L. Han, P. Wang and S. Dong, *Nanoscale*, 2012, **4**, 5814.
[19] S. Q. Liu, Z. Chen, N. Zhang, Z. R. Tang and Y. J. Xu, *J. Phys. Chem. C*, 2013, **117**, 8251.
[20] Q. Xiang and J. Yu, *J. Phys. Chem. Lett.*, 2013, **4**, 753.
[21] M. Q. Yang and Y. J. Xu, *Phys. Chem. Chem. Phys.*, 2013, **15**, 19102.
[22] Y. H. Zhang, Z. R. Tang, X. Z. Fu and Y. J. Xu, *ACS nano*, 2011, **5**, 7426.
[23] C. Han, M. Q. Yang, B. Weng and Y. J. Xu, *Phys. Chem. Chem. Phys.*, 2014, **16**, 16891.
[24] M. Q. Yang, N. Zhang, M. Pagliaro and Y. J. Xu, *Chem. Soc. Rev.*, DOI: 10.1039/c4cs00213j.
[25] J. Wang, C. An, J. Liu, G. Xi, W. Jiang, S. Wang and Q. Zhang, *J. Mater. Chem. A*, 2013, **1**, 2827.
[26] P. Wang, Y. Zhai, D. Wang and S. Dong, *Nanoscale*, 2011, **3**, 1640.
[27] D. W. Hwang, H. G. Kim, J. Kim, K. Y. Cha, Y. G. Kim and J. S. Lee, *J. Catal.*, 2000, **193**, 40.
[28] H. Kim, D. Hwang, Y. Kim and J. Lee, *Chem. Commu.*, 1999, 1077.
[29] M. M. Milanova, M. Kakihana, M. Arima, M. Yashima and M. Yoshimura, *J. Alloys Compd.*, 1996, **242**, 6.
[30] K. Onozuka, Y. Kawakami, H. Imai, T. Yokoi, T. Tatsumi and J. N. Kondo, *J. Solid State Chem.*, 2012, **192**, 87.
[31] K. W. Li, Y. Wang, H. Wang, M. Zhu and H. Yan, *Nanotechnology*, 2006, **17**, 4863.
[32] C. H. Wu, Y. Z. Zhang, S. Li, H. J. Zheng, H. Wang, J. B. Liu, K.W. Li and H. Yan, *Chem. Eng. J.*, 2011, **178**, 468.
[33] M. Q. Yang, B. Weng and Y. J. Xu, *Langmuir*, 2013, **29**, 10549.
[34] J. S. Lee, K. H. You and C. B. Park, *Adv. Mater.*, 2012, **24**, 1084.
[35] X. J. Bai, L. Wang, R. L. Zong, Y. H. Lv, Y. Q. Sun and Y. F. Zhu, *Langmuir*, 2013, **29**, 3097.
[36] X. Yan, Y. J. Li, F. Du, K. Zhu, Y. Q. Zhang, A. Y. Su, G. Chen and Y. J. Wei, *Nanoscale*, 2014, **6**, 4108 .
[37] O. Akhavan, *ACS Nano*, 2010, **4**, 4174.
[38] Y. Y. Bu, Z. Y. Chen, W. B. Li and B. R. Hou, *ACS Appl. Mater. Interfaces*, 2013, **5**, 12361.
[39] C. H. Wu, Y. Z. Zhang, S. Lia, H. J. Zheng, H. Wang, J. B. Liu, K. W. Li and H. Yan, *Chem. Eng. J.*, 2011, **178**, 468.
[40] S. J. Hu, L. C. Jia, B. Chi, J. Pu and J. Li, *J. Power Sources*, 2014, **6**, 304.
[41] S. J. Hu, B. Chi, J. Pu and J. Li, *J. Mater. Chem. A*, 2014, DOI: 10.1039/C4TA04177A.
[42] D. W. Hwang, H. G. Kim, J. S. Jang, S. W. Bae, S. M. Ji and J. S. Lee, *Catal. Today*, 2004, **93−95**, 845.
[43] W. S. Hummers and R. E. Offeman, *J. Am. Chem. Soc.*, 1958, **80**, 1339.
[44] C. Nethravathi and M. Rajamathi, *Carbon*, 2008, **46**, 1994.
[45] L. Yuan, M. Q. Yang and Y. J. Xu, *Nanoscale*, 2014, **6**, 6335.
[46] A. A. Ismail and D. W. Bahnemann, *J. Phys. Chem. C*, 2011, **115**, 5784.
[47] M. S. Zhu, Z. Li, B. Xiao, Y. T. Lu, Y. K. Du, P. Yang and X. M. Wang, *ACS Appl. Mater. Interfaces*, 2013, **5**, 1732.
[48] Q. Xiang, J. Yu and M. Jaroniec, *J. Am. Chem. Soc.*, 2012, **134**, 6575.
[49] N. Jiang, Z. L. Xiu, Z. Xie, H. Y. Li, G. Zhao, W. P. Wang, Y. Z. Wu and X. P. Hao, *New J. Chem.*, 2014, **38**, 4312.
[50] V. Bessergenev, R. Pereira, M. Mateus, I. Khmelinskii, D. Vasconcelos, R. Nicula, E. Burkel, A. Botelho do Rego and A. Saprykin, *Thin Solid Films*, 2006, **503**, 29.
[51] M. Sunding, K. Hadidi, S. Diplas, O. Løvvik, T. Norby and A. Gunnæs, *J. Electron. Spectrosc. Relat. Phenom.*, 2011, **184**, 399.
[52] S. Bouattour, A. M. Botelho do Rego and L. F. Vieira Ferreira, *Mater. Res. Bull.*, 2010, **45**, 818.
[53] H. He, T. Riedl, A. Lerf and J. Klinowski, *J. Phys. Chem.*, 1996, **100**, 19954.
[54] C. Gó mez−Navarro, R. T. Weitz, A. M. Bittner, M. Scolari, A. Mews, M. Burghard and K. Kern, *Nano Lett.*, 2007, **7**, 3499.
[55] S. Stankovich, D. A. Dikin, R. D. Piner, K. A. Kohlhaas, A. Kleinhammes, Y. Jia, Y. Wu, S. T. Nguyen and R. S. Ruoff, *Carbon*, 2007, **45**, 1558.
[56] S. Chen, J. Zhu and X. Wang, *J. Phys. Chem. C*, 2010, **114**, 11829.
[57] T. Nakajima, A. Mabuchi and R. Hagiwara, *Carbon*, 1988, **26**, 357.
[58] H. L. Guo, X. F. Wang, Q. Y. Qian, F. B. Wang and X. H. Xia, *ACS Nano*, 2009, **3**, 2653.
[59] C. Nethravathi and M. Rajamathi, *Carbon*, 2008, **46**, 1994.
[60] M. S. Zhu, Y. K. Du, P. Yang and X. Wang, *Catal. Sci. Technol.*, 2013, **3**, 2295.
[61] C. Y. Zhai, M. S. Zhu, Y. T. Lu, F. F. Ren, C. Q. Wang, Y. K. Du and P. Yang, *Phys. Chem. Chem. Phys.*, 2014, **16**, 14800.
[62] N. Zhang, M. Q. Yang, Z. R. Tang and Y. J. Xu, *ACS nano*, 2014, **8**, 623.
[63] S. Q. Liu, M. Q. Yang and Y. J. Xu, *J. Mater. Chem. A*, 2014, **2**, 430.